Chinese Chemical Letters 35 (2024) 109032

Contents lists available at ScienceDirect

Chinese Chemical Letters

journal homepage: www.elsevier.com/locate/cclet

Theoretical and experimental cocrystal screening of temozolomide with a series of phenolic acids, promising cocrystal coformers

Hongmei Yu[a,1], Baoxi Zhang[a,1], Meiju Liu[a], Cheng Xing[a], Guorong He[b], Li Zhang[a], Ningbo Gong[a,*], Yang Lu[a,*], Guanhua Du[b]

[a] Beijing Key Laboratory of Polymorphic Drugs, Institute of Materia Medica, Chinese Academy of Medical Sciences and Peking Union Medical College, Beijing 100050, China
[b] Beijing City Key Laboratory of Drug Target Identification and Drug Screening, Institute of Materia Medica, Chinese Academy of Medical Sciences and Peking Union Medical College, Beijing 100050, China

ARTICLE INFO

Article history:
Received 16 February 2023
Revised 1 August 2023
Accepted 31 August 2023
Available online 4 September 2023

Keywords:
Virtual
Cocrystal
Temozolomide
Supramolecular synthon
Phenolic acid
Stability

ABSTRACT

The virtual cocrystal screening approach based on molecular electrostatic potential surface (MEPS) maps is a fast and feasible computational method to estimate the probability of cocrystal formation by calculating the difference in the interaction site pairing energies of monomers and that of their assemblies prior to experimental screening. In this paper, we report 12 cocrystal forms of temozolomide with mono-, di-, and trihydroxy benzoic acids, namely, 3–hydroxy-, 2,4-dihydroxy-, 2,5-dihydroxy-, 2,6-dihydroxy-, 3,4-dihydroxy-, and 3,4,5-trihydroxy-benzoic acids, as well as benzoic acid, as pharmaceutical coformers for the first time. 10 single crystals out of the 12 cocrystal forms were obtained and unequivocally determined by single-crystal X-ray diffraction, which clarified spatial arrangements, molecular conformations, and supramolecular synthons. MEPS further gains some insights into the sites of hydrogen bonding interactions for exploring combination patterns in these assemblies. Modulated stability of TMZ was successfully achieved by cocrystallization with these acids.

The past decades have seen an explosion of progress in the development of pharmaceutical cocrystals, which have evolved as a reliable tool to fine-tune the physicochemical properties of APIs [1–5]. However, in many cases, cocrystallization sometimes results in serendipitous products, such as polymorphs, solvates, and hydrates of multi-component or single-component crystals, which inadvertently occurs during API processing and formulation and poses challenges to the quality and performance control of the drug product [6–10]. Therefore, it needs special attention to investigate the formation of solvates/hydrates, the desolvation/dehydration processes, and the polymorphic behaviors of cocrystals. The knowledge gained can help avoid unintentional solvates/hydrates or polymorphs formed during crystallization, and control the generation of desired forms by altering the parameters during crystallization experiments in the pharmaceutical industries.

Temozolomide (8-carbamoyl-3-methylimidazo[5,1-*d*]-1,2,3,5-tetrazin-4(3*H*)-one, TMZ, Scheme 1) is an oral alkylating agent against malignant gliomas [11]. There is a disadvantage of poor stability of TMZ, as it degrades into 5-aminoimidazole-4-carboxamide (AIC) during storage and processing, which would lead to reduced therapeutic efficacy [12,13]. Investigations of TMZ cocrystals with succinic acid and oxalic acid have already seen significantly improved stability and potential in pharmaceutical applicability [14]. These previous works encourage us to design and develop novel solid forms of TMZ, aiming to gain better stability of this pristine drug without changing its chemical structure.

TMZ cocrystals are rationally designed by selecting benzoic acid and its hydroxyl derivatives as cocrystal coformers (CCFs) based on the following considerations. On the one hand, the principle of supramolecular synthon [15,16] in crystal engineering helps to guide cocrystal design. The amide group and tetrazine N atoms on TMZ are promising hydrogen bond acceptors, which renders TMZ a suitable candidate for modulating its physicochemical properties through cocrystallization. In this respect, a series of mono-, di-, and tri-hydroxybenzoic acids as well as benzoic acid with good proton donors (hydroxyl and carboxyl groups) were selected as promising CCFs for cocrystal constructions. On the other hand, studies have previously shown that TMZ is stable at pH < 5 but labile at pH > 7 [17]. The hydrolytic degradations of TMZ to AIC

* Corresponding authors.
E-mail addresses: gnb@imm.ac.cn (N. Gong), luy@imm.ac.cn (Y. Lu).
[1] These authors contributed equally to this work.

https://doi.org/10.1016/j.cclet.2023.109032
1001-8417/

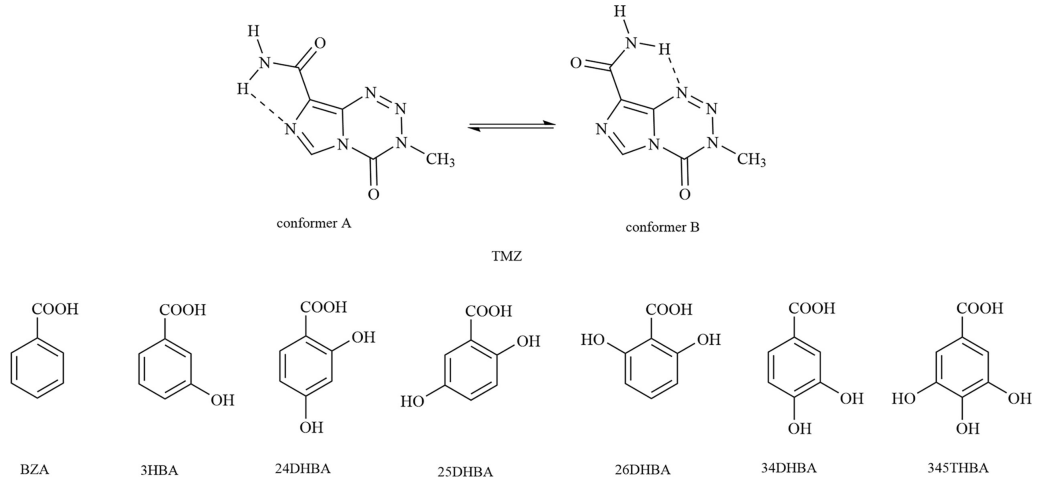

Scheme 1. Chemical structures of temozolomide (TMZ, conformers A and B) and cocrystal coformers (CCFs) used in this study.

could be inhibited by employing acid partners (pK_a range of 1∼5) as pH adjusters [14]. Furthermore, hydroxybenzoic acids were selected from the generally regarded as safe (GRAS) compound list approved by Food and Drug Administration [18] with excellent anti-oxidant properties [19]. Hunter's virtual cocrystal screening method [20–22] by using molecular electrostatic potential surfaces (MEPS) based on density functional theory (DFT) was implemented in this study to predict the probability of cocrystal formation between TMZ (conformers A and B) and these acids. We report herein, 12 novel solid forms, TMZ-BZA (1:1, **S1**), TMZ-3HBA (1:1, **S2**), TMZ-24DHBA-MeOH (1:1:1, **S3**), TMZ-24DHBA (1:1 form A, **S4**), TMZ-24DHBA (1:1 form B, **S5**), TMZ-24DHBA (2:1, **S6**), TMZ-25DHBA-MeOH (1:1:1, **S7**), TMZ-25DHBA-H_2O (1:1:1, **S8**), TMZ-25DHBA (1:1, **S9**), TMZ-26DHBA (1:1, **S10**), TMZ-34DHBA (1:1, **S11**), TMZ-345THBA-H_2O (3:1:1, **S12**) for the first time. The results show that the prediction results are in good agreement with the experimental screening ones. The various supramolecular synthons formed by TMZ and CCFs in the crystal lattice of cocrystals responsible for the arrangement of molecules were specified by single-crystal X-ray diffraction (SCXRD). Powder products synthesized by the slurry method were characterized and confirmed by powder X-ray diffraction (PXRD) measurements together with differential scanning calorimetry (DSC), thermogravimetric analysis (TGA), and Fourier transform infrared spectroscopy (FT-IR) analysis.

TMZ raw material (form 1, same as CSD refcode DIPGIS10 [23], BZA (98%), 3HBA (98%), 24DHBA (98%), 25DHBA (98%), 26DHBA (98%), 34DHBA (98%), and 345THBA monohydrate (98%) were purchased from Hubei Wande Chemical Co., Ltd., (Wuhan, China). All chromatographical-grade solvents were purchased from Sigma Aldrich (St. Louis, MO, USA). All analytical-grade solvents were purchased from Beijing Chemical Works (Beijing, China).

TMZ cocrystal powders were prepared by the slurry method. Taking **S1** as an example, TMZ and BZA in a ratio of 1:1 were suspended in ethanol solution. The suspension was agitated at 400 r/min for 24 h at 25 °C, followed by filtration of the agglomerates. The powder samples were dried in a vacuum drying oven (DZF-6020) at 40 °C for 6 h. The same steps were applied to prepare other TMZ-hydroxybenzoic acid cocrystals in a definite ratio using corresponding suitable solvents. Unfortunately, the cocrystal powders of **S12** were not obtained despite many attempts.

The diffraction-quality single crystals were obtained by the solvent evaporation method. The single crystal of **S1** was obtained by dissolving 50 mg of a stoichiometric 1:10 mixture of the components in 10 mL of methanol:ethyl acetate (1:1) followed by sonication for complete dissolution. Then, the clear solution was filtered and covered with Parafilm pierced with a few small holes, and left for slow evaporation. Approximately 7 days later, suitable crystals precipitated out of the solution. The same steps were applied for the harvest of other TMZ-hydroxybenzoic acid crystals. Attempts to grow single crystals of **S5** and **S9** from different solvents were unsuccessful. Detailed synthesis conditions of slurry and solution crystallization methods for 12 cocrystal forms are given in Table S1 (Supporting information).

SCXRD experiments were performed at 295 K on a Rigaku Micromax 002+ diffractometer (USA) using Cu *Kα* radiation (λ = 1.54187 Å), equipped with a CCD detector and a graphite monochromator (Rigaku, Americas, The Woodlands, TX, USA). The structures were solved *via* the direct method by SHELXT-2018/2 [24], and refinements were carried out by the full-matrix least-squares method against F^2 using SHELXL-2018/3 [25]. Anisotropic displacement parameters were applied for non-hydrogen atoms. Generally, hydrogen atoms bonded to nitrogen or oxygen were located from the difference electron density maps. Other hydrogen atoms were placed in their calculated positions and refined using a riding model.

The DFT calculations were carried out with a Gaussian 16 W package to calculate the quantum parameters and optimize the molecular geometry of TMZ, CCFs (BZA, 3HBA, 24DHBA, 25DHBA, 26DHBA, 34DHBA, 345THBA) at the B3LYP/6-311G (d, p) level [26,27]. The maxima and minima sites were plotted on the MEPS isosurface (0.001 a.u. electron density isosurface), generated by the Multiwfn 3.8 package and visualized by the VMD 1.9.4 package [28,29].

PXRD data collection was accomplished on a D/max-2550 (Rigaku, Tokyo, Japan) X-ray diffractometer with Cu *Kα* radiation (λ = 1.54178 Å) as a source. The tube voltage and amperage of the generator were set to 40 kV and 150 mA, respectively. Data over the 2θ range of 3°−40° was collected with a scan speed of 8°/min (step size 0.02°). The program Mercury (version 2020.3.0, Cambridge Crystallographic Data Center, Cambridge, UK) was used for the generation of simulated PXRD patterns based on the SCXRD data, and data were further analyzed using Jade 6.5 software.

The DSC experiments were performed on a Mettler Toledo DSC1 Instrument (Greifensee, Switzerland) under the air gas. Samples weighing 2–4 mg were heated in sealed aluminum pans from 30 °C to 220 °C with a heating rate of 10 °C/min.

TGA was performed on a Mettler-Toledo TGA/DSC1 STARe instrument (Greifensee, Switzerland) under the nitrogen gas purge (50 mL/min). Samples weighing 4–6 mg were placed in an Al_2O_3 crucible and heated from 30 °C to 500 °C with a heating rate of

Table 1
pK_a values, melting points of all CCFs, decomposition peaks of corresponding cocrystals, and the difference in the interaction site pairing energies (ΔE) values of isolated monomers and that of cocrystals.

Compound	pK_a (-COOH)	CCF melting points (°C)	Cocrystal decomposition peaks (°C)	ΔE (kJ/mol)	
				TMZ (conformer A)	TMZ (conformer B)
BZA	4.20	124.06	179.87	−6.38	−6.95
2HBA	2.97	160.29	174.98	−11.87	−13.04
3HBA	4.08	203.66	187.10	−9.97	−10.38
24DHBA	3.10	226.59	198.57, 199.59, 198.95, 201.55	−13.67	−14.66
25DHBA	2.53	203.60, 207.19	193.97, 193.74, 197.55	−9.94	−10.73
26DHBA	1.64	169.30	179.99	−10.14	−11.03
34DHBA	4.48	203.76	199.96	−12.60	−13.00
345THBA	4.50	266.05	–	−15.69	−15.96

10 °C /min. All DSC and TGA thermograms were analyzed and imaged using the STARe software.

FT-IR spectra were collected by a PerkinElmer FT-IR 400 spectrometer in the range of 4000–650 cm^{-1}, with a resolution of 4 cm^{-1} under ambient conditions (Table S2 in Supporting information).

Accelerated stability tests were carried out according to General Rule 9001 of the fourth part of Chinese Pharmacopoeia to evaluate the physical stability of cocrystals in comparison with the pure drug. Powdered samples of TMZ cocrystals (**S1**-**S11**) were stored at elevated temperature (60 ± 1 °C) and humidity (90% ± 5%, 25 °C) for 3 months. Periodically (1 month, 2 months, 3 months), samples were removed from instruments for physical examinations, PXRD, and HPLC measurements to detect the color change, solid-state phase stability, and chemical stability, respectively.

Phase transformations of four polymorphic forms of TMZ-24DHBA and three polymorphic forms of TMZ-25DHBA were conducted by using slurry, heating, and grinding methods to determine the thermodynamically stable form and phase transition processes.

It is always favorable to select the potential CCFs beforehand to make the development process of supramolecular assemblies more efficient. Structurally speaking, considering the amide group and tetrazine ring of TMZ and the high persistence of carboxylic···amide and O-H···Narom synthons in cocrystals, we were encouraged to investigate the possibility of TMZ cocrystallization with a series of benzoic acid with/without hydroxyl substituent groups in different numbers and positions. We would like to see whether a slight change in structures would make a difference in the cocrystallization results.

A fast and feasible virtual cocrystal screening approach has been developed by Hunter *et al.* [20] to estimate the possibility of cocrystal formation. The interaction site pairing energy for each contact, $-\alpha_i\beta_j$, is calculated using α_i and β_j H-bond parameters determined from maxima and minima on the MEPS, and the total interaction site pairing energy, *E*, of the solid is estimated as the sum overall contacts. The difference in the interaction site pairing energies between two pure components and cocrystals, defined as ΔE, is given as an evaluation of the possibility of cocrystal formation. The smaller the value of ΔE, the more probable the cocrystal formation, with the threshold of −11 kJ/mol indicating a more than 50% probability of a given cocrystal. The pK_a values and the difference in the interaction site pairing energies (ΔE) values of isolated monomers and that of their assemblies between TMZ and CCFs have been presented in Table 1. It is clear from Table 1 that the obtained ΔE values are smaller than −11 for at least one conformation of TMZ with 2HBA, 24DHBA, 34DHBA, and 345THBA, which suggests a high possibility of cocrystal formation. Since the ΔE values of 3HBA and 25DHBA are very close to the threshold, we speculate that there is still a good chance of cocrystal formation. Collectively, the structural traits, safe and acidic characteristics, and energetic preferability of these benzoic acid hydroxyl–derivatives enable them ideal candidates as CCFs to cocrystallize with TMZ.

Experimental cocrystal screening with BZA, 3HBA, 24DHBA, 25DHBA, 26DHBA, 34DHBA, and 345THBA produced 12 cocrystal forms, among which, TMZ-24DHBA exhibits in four forms and TMZ-25DHBA were observed to exist in three forms. Out of 12 TMZ cocrystal forms, 10 crystals were harvested, the structures of which were confirmed by SCXRD. The crystallographic parameters for structures are presented in Table 2 and hydrogen bond geometrical parameters are provided in Table S2 (Supporting information). To make information about the structural parameters clear and understandable, asymmetric units with atom labeling schemes of all 10 structures are given in Fig. S1 (Supporting information). The CIF and checkcif files have been deposited in the Cambridge Structural Database (CCDC numbers 2240451-2240460). The main hydrogen bonding motifs in these crystal structures, as well as conformations of TMZ would be discussed below and summarized in Table 3.

TMZ-BZA (3:3), ***S1***: It was solved in the triclinic space group *P* -1 ($Z = 2$) with three molecules of TMZ (conformer A, suffix with A, B, C) and three molecules of BZA (suffix with A, B, C) in the asymmetric unit ($Z' = 1$). Two-point robust acid-amide heterodimers are formed between molecules A and C of TMZ and molecules A and C of BZA (O_3-H_{3A}···O_{2A}: 2.588 Å, N_{6A}-H_{6AA}···O_{4A}: 2.953 Å; O_{3C}-H_{3C}···O_{2C}: 2.551 Å, N_{6C}-H_{6CA}···O_{4C}: 3.016 Å), leading to the formation of dimers. Two adjacent dimers interconnected through N_{6C}-H_{6CB}···O_{4A}: 2.994 Å, N_{6A}-H_{6AB}···O_{4C}: 3.016 Å hydrogen bonds, giving a cyclic tetrameric ring. Notably, these tetrameric units further self-assembled and extended *via* weak hetero-synthons (C_{4A}-H_{4A}···O_{1C}: 3.317 Å, C_{4C}–H_{4C}···O_{1A}: 3.259 Å) between TMZ molecules A and C, resulting in a two-dimensional (2D) approximately planar sheet (composed by TMZ and BZA molecules A and C). Similarly, acid-amide heterodimer (O_{3B}-H_{3B}···O_{2B}: 2.565 Å, N_{6B}-H_{6BA}···O_{4B}: 2.983 Å) and N_{6B}-H_{6BB}···O_{4B}: 2.980 Å hydrogen bond between molecules B of TMZ and BZA also exist, forming the second layer (composed by TMZ and BZA molecules B). The two adjacent layers are further packed by π-π stacking, as well as van der Waals forces and other weak contacts to generate a 3D layered structure (Fig. 1a).

TMZ-3HBA (1:1), ***S2***: It crystallized in the monoclinic space group *C*2/*c* ($Z = 8$) with one molecule each of TMZ (conformer A) and 3HBA in the asymmetric unit ($Z' = 1$). Primary supramolecular synthon is the acid-amide hetero-synthon (O_3-H_3···O_2: 2.656 Å and N_6-H_{6A}···O_4: 2.969 Å) involving the carboxyl group of 3HBA and amide group of TMZ, leading to a heterodimer. The two adjacent supramolecular dimers are connected through a centrosymmetric homo-synthon (C_4-H_4···O_1: 3.150 Å) between the imidazolyl C-H group of TMZ and the O atom of the carbonyl group of neighboring TMZ molecule, extending to an infinite hydrogen-bonded chain. Such chains are further interconnected in a crossed style through N_6-H_{6B}···O_4: 2.928 Å, O_5-H_5···N_4: 2.879 Å hydrogen bonds, lead-

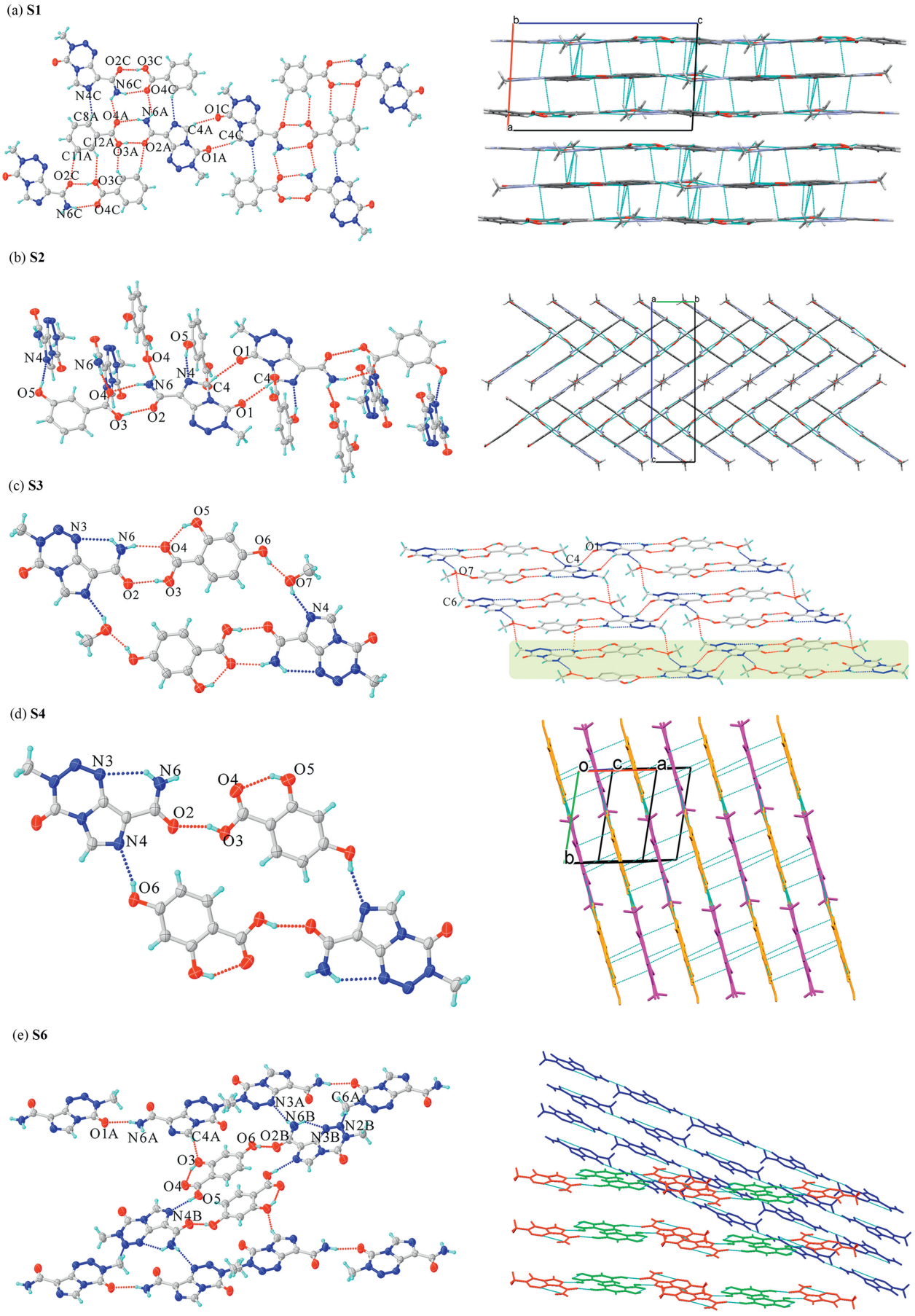

Fig. 1. (a-e) Hydrogen-bonded motifs (left), and the 3D packing structure of the cocrystals **S1**-**S6** (right).

Table 2
Crystallographic information and structure refinement parameters for TMZ cocrystals.

Parameters	**S1**	**S2**	**S3**	**S4**	**S6**
Formula	$3(C_6H_6N_6O_2)$, $3(C_7H_6O_2)$	$C_6H_6N_6O_2$, $C_7H_6O_3$	$C_6H_6N_6O_2$, $C_7H_6O_4$, CH_4O	$C_6H_6N_6O_2$, $C_7H_6O_4$	$2(C_6H_6N_6O_2)$, $C_7H_6O_4$
Formula weight	948.86	332.29	380.33	348.29	542.45
Crystal size (mm)	0.13 × 0.17 × 0.35	0.09 × 0.28 × 0.38	0.01 × 0.05 × 0.33	0.02 × 0.11 × 0.36	0.12 × 0.12 × 0.34
Description	Block	Plate	Needle	Needle	Column
Crystal system	Triclinic	Monoclinic	Triclinic	Triclinic	Triclinic
Space group	*P* - 1	*C*2/*c*	*P* - 1	*P* - 1	*P* - 1
a (Å)	10.812 (1)	24.293 (1)	7.108 (1)	7.205 (1)	6.983 (1)
b (Å)	12.360 (1)	5.620 (1)	9.894 (1)	8.162 (1)	9.667 (1)
c (Å)	17.114 (1)	20.848 (1)	12.634 (1)	12.820 (1)	18.103 (1)
α (°)	94.86 (1)	90	93.30 (1)	102.87 (1)	97.58 (1)
β (°)	90.78 (1)	93.02 (1)	98.45 (1)	98.03 (1)	94.75 (1)
γ (°)	113.49 (1)	90	109.48 (1)	95.39 (1)	109.96 (1)
Volume (Å^3)	2087.16 (14)	2842.14 (7)	823.10 (6)	721.70 (8)	1127.75 (6)
Z/*Z*′	2/1	8/1	2/1	2/1	2/1
Density (g/cm^3)	1.510	1.553	1.535	1.603	1.597
Independent reflections	7915	2743	3133	2716	4279
Reflections with $I > 2\sigma(I)$	6298	2503	2658	2238	3815
Final R, w$R(F^2)$ value [$I > 2\sigma(I)$]	0.085, 0.230	0.056, 0.159	0.072, 0.199	0.095, 0.286	0.057, 0.156
GOF	1.076	1.048	1.054	1.022	1.071
R_{int}	0.0417	0.0594	0.0643	0.0757	0.0478
CCDC number	2240,451	2240,452	2240,453	2240,454	2240,455
Parameters	**S7**	**S8**	**S10**	**S11**	**S12**
Formula	$C_6H_6N_6O_2$, $C_7H_6O_4$, CH_4O	$C_6H_6N_6O_2$, $C_7H_6O_4$, H_2O	$C_6H_6N_6O_2$, $C_7H_6O_4$	$C_6H_6N_6O_2$, $C_7H_6O_4$	$3(C_6H_6N_6O_2)$, $C_7H_6O_4$, H_2O
Formula weight	380.33	366.30	348.29	348.29	770.64
Crystal size (mm)	0.09 × 0.15 × 0.29	0.10 × 0.20 × 0.30	0.15 × 0.28 × 0.46	0.10 × 0.15 × 0.46	0.11 × 0.15 × 0.36
Description	Column	Column	Plate	Plate	Plate
Crystal system	Triclinic	Triclinic	Monoclinic	Triclinic	Monoclinic
Space group	*P* - 1	*P* - 1	*I*2/*m*	*P* - 1	*Pc*
a (Å)	6.881 (1)	6.829 (1)	14.156 (1)	7.815 (1)	17.556 (1)
b (Å)	9.964 (1)	9.969 (1)	6.516 (1)	9.285 (1)	7.321 (1)
c (Å)	12.867 (1)	12.240 (1)	16.174 (1)	10.990 (1)	13.340 (1)
α (°)	80.60 (1)	72.06 (1)	90	110.40 (1)	90
β (°)	78.59 (1)	85.46 (1)	100.18 (1)	95.38 (1)	111.47 (1)
γ (°)	72.17 (1)	74.56 (1)	90	97.69 (1)	90
Volume (Å^3)	818.31 (5)	764.20 (4)	1468.43 (4)	732.23 (4)	1595.73 (4)
Z/*Z*′	2/1	2/1	4/0.5	2/1	2/1
Density (g/cm^3)	1.544	1.592	1.575	1.580	1.604
Independent reflections	3321	2910	1560	2812	5329
Reflections with $I > 2\sigma(I)$	2835	2725	1522	2673	5002
Final R, w$R(F^2)$ value [$I > 2\sigma(I)$]	0.040, 0.113	0.039, 0.109	0.037, 0.104	0.036, 0.103	0.038, 0.100
GOF	1.060	1.053	1.062	1.037	1.055
R_{int}	0.0482	0.0339	0.0193	0.0202	0.0423
CCDC number	2240,456	2240,457	2240,458	2240,459	2240,460

Table 3
Predominant synthons, stoichiometry, and conformers of TMZ in the crystal structures.

No.	Crystal structure	Stoichiometry	Predominant synthons	Conformer
S1	TMZ-BZA	1:1	1 + 7	A
S2	TMZ-3HBA	1:1	1 + 7 + 11	A
S3	TMZ-24DHBA-MeOH	1:1:1	1 + 11	B
S4	TMZ-24DHBA	1:1	8 + 11	B
S6	TMZ-24DHBA	2:1	5 + 6 + 9 + 10	A + B
S7	TMZ-25DHBA-MeOH	1:1:1	1 + 11	B
S8	TMZ-25DHBA-H_2O	1:1:1	1 + 11+12	B
S10	TMZ-26DHBA	1:1	4 + 10	A
S11	TMZ-34DHBA	1:1	3 + 9 + 10	A
S12	TMZ-345THBA-H_2O	3:1:1	2 + 7 + 10+13	A

ing to the formation of a herringbone-like 3D architecture viewed down the crystallographic a-axis (Fig. 1b).

TMZ-24DHBA-MeOH (1:1:1), ***S3***: During cocrystallization of TMZ with 24DHBA, four polymorphic forms including a methanolate, two forms (form A and B) in the ratio of 1:1, and a 2:1 form were obtained. The TMZ-24DHBA-MeOH form was crystallized from methanol solvent and was solved in the triclinic space group *P* - 1 ($Z = 2$), with an asymmetric unit consisting of one TMZ (conformer B), one 24DHBA, and one methanol molecule ($Z' = 1$). The intramolecular hydrogen bond is observed within TMZ conformer B (N_6-$H_{6B}\cdots N_3$: 2.980 Å) and 24DHBA molecule (O_5-$H_5\cdots O_4$: 2.563 Å). The main interaction governing the cocrystal formation is the

acid-amide hetero-synthon (O_3-H_3···O_2: 2.655 Å and N_6-H_{6A}···O_4: 2.855 Å) involving the carboxyl group of 24DHBA and TMZ amide and O_6-H_6···O_7: 2.589 Å hydrogen bond between methanol and 24DHBA, constituting a trimetric unit. At the same time, the methanol molecule plays the "linkage" role with the TMZ molecule *via* O_7-H_7···N_4: 2.838 Å, leading to the formation of a rectangular six-member assembly. These assemblies repeat and extend to give an infinite 2D ribbon, and then are arranged into a 3D stair-like structure (Fig. 1c).

TMZ-24DHBA (1:1) Form A, ***S4***: Solvent evaporation in ethanol solution gave crystals of TMZ-24DHBA (1:1) Form A. It belongs to the triclinic system *P* - 1 space group ($Z=2$). Each asymmetric unit consists of one TMZ (conformer B) and one 24DHBA molecule ($Z'=1$). Like **S3**, there also exists an intramolecular N_6-H_{6B}···N_3: 2.995 Å hydrogen bond within TMZ molecule and O_5-H_5···O_4: 2.643 Å hydrogen bond within 24DHBA molecule. However, robust acid-amide hetero-synthon is not present in this structure, while the carboxylic hydroxyl group of 24DHBA interacts with TMZ amide carbonyl through O_3-H_3···O_2: 2.590 Å. The dimer of TMZ and 24DHBA is connected *via* O_6-H_6···N_4: 2.878 Å hydrogen bond, leading to a tetramolecular unit. These units further stack into a 3D layered structure sustained by van der Waals forces and other weak contacts (Fig. 1d).

TMZ-24DHBA (2:1), ***S6***: Solvent volatilization in the mixed solvent of ethanol and acetonitrile (1:1, v:v) gave the polymorphic form of TMZ-24DHBA (2:1). It was solved in triclinic system *P* - 1 space group ($Z=2$) with two molecules of TMZ (conformer A and B) and one molecule of 24DHBA in the asymmetric unit ($Z'=1$). There exists an intramolecular hydrogen bond N_{6B}-H_{6BB}···N_{3B}: 3.017 Å within TMZ conformer B and O_3-H_3···O_4: 2.575 Å hydrogen bond within the 24DHBA molecule. Primary interactions between 24DHBA and TMZ conformer B are O_5-H_5···N_{4B}: 2.732 Å and O_6-H_6···O_{2B}: 2.728 Å hydrogen bonds, leading to the formation of a quaternion ring unit composed of two 24DHBA and two TMZ conformer B molecules, further building a 2D sheet arranged in a parallel way. On the other side, the TMZ conformer A molecule connects adjacent one *via* N_{6A}-H_{6AA}···O_{1A}: 2.939 Å hydrogen bond and is arranged into chains in a parallel array. The units of 24DHBA and TMZ conformer B connect with TMZ conformer A through C_{4A}-H_{4A}···O_3: 3.187 Å, N_{6B}-H_{6BA}···N_{3A}: 3.180 Å, and C_{6A}-H_{6AC}···N_{2B}: 3.306 Å hydrogen bonds. The two sets of layered sheets are then fitted into 3D architecture in an overlapping way (Fig. 1e).

TMZ-25DHBA-MeOH (1:1:1), ***S7***: Slow evaporation of TMZ and 25DHBA gave a methanolate form and a monohydrate form of TMZ-25DHBA. The TMZ-25DHBA-MeOH form was crystallized from methanol solvent and was solved in the triclinic space group *P* - 1 ($Z=2$), with each molecule of TMZ (conformer B), 25DHBA, and methanol in the asymmetric unit ($Z'=1$). Resembling that of **S3**, the carboxyl group of 25DHBA interacts with TMZ amide through hetero-synthon (O_3-H_3···O_2: 2.646 Å and N_6-H_{6A}···O_4: 2.881 Å), and connects with methanol by O_6-H_6···O_7: 2.694 Å hydrogen bond, resulting in a ternary motif. At the same time, methanol molecules were involved in linking the adjacent trimers through the O_7-H_7···N_4: 2.854 Å hydrogen bond, leading to the formation of a six-member rectangular network, which further extend and create a 3D layered structure viewed down b axis (Fig. 2a).

TMZ-25DHBA-H_2O (1:1:1), ***S8***: The TMZ-25DHBA-H_2O cocrystal was crystallized from ethanol solvent and was solved in the triclinic space group *P* - 1 ($Z=2$), with one molecule of TMZ (conformer B), one molecule of 25DHBA, and one water molecule in the asymmetric unit ($Z'=1$). Resembling that of **S3** and **S7**, the carboxyl group of 25DHBA interacts with TMZ amide through an acid-amide hetero-synthon (O_3-H_3···O_2: 2.605 Å and N_6-H_{6A}···O_4: 2.914 Å), and the water molecule is engaged in O_6-H_6···O_7: 2.643 Å hydrogen bond connecting with 25DHBA, constituting a trimer. A rectangular hexamer is formed mediated by O_7-H_{7A}···N_4 hydrogen bond involving two trimers. Two adjacent six-member units are held together *via* O_7-H_{7B}···O_1 hydrogen bonds, which extend into an infinite tape, and further stacked into a stair-like layered 3D architecture *via* relatively weak interactions (Fig. 2b).

TMZ-26DHBA (1:1), ***S10***: It crystallized in the monoclinic space group *I*2/*m* ($Z=4$) with one molecule each of TMZ conformer A and 26DHBA in the asymmetric unit ($Z'=0.5$). Two intramolecular interactions were observed within 26DHBA molecules (O_3-H_3···O_6: 2.528 Å, O_5-H_5···O_4: 2.596 Å). The acid-amide heterodimer is not present in this structure. The carboxyl group of 26DHBA interacts with TMZ through O_6-H_6···O_2: 2.602 Å. The hydrogen-bonded motif of one TMZ and one 26DHBA molecule is connected to another *via* a C_4-H_4···O_4: 3.214 Å hydrogen bond, and a centrosymmetric homo-synthon (N_6-H_{6B}···N_4: 3.091 Å) formed between two neighboring TMZ molecules. These units adopt perfectly planar conformation and repeat into linear polymer chains parallel to the crystallographic a-axis, thus forming a 3D paralleled layer-like structure (Fig. 2c).

TMZ-34DHBA (1:1), ***S11***: It crystallized in the triclinic space group *P* - 1 ($Z=2$) with one molecule of TMZ conformer A and one molecule of 34DHBA in the asymmetric unit ($Z'=1$). In the asymmetric unit, 34DHBA interacts with TMZ through O_6–H_6···O_2: 2.569 Å involving the hydroxyl group of 34DHBA and amide carbonyl of TMZ. The dimers were repeated and extended *via* a centrosymmetric homo-synthon (O_5–H_5···O_6: 2.766 Å) between two adjacent 34DHBA molecules and O_3-H_3···N_4: 2.799 Å hydrogen bond involving the hydroxyl group of 34DHBA and imidazole N_4 atom of TMZ. The 3D layered structure is formed thanks to C-H···O weak interactions between adjacent stacks (Fig. 2d).

TMZ-345THBA-H_2O (3:1:1), ***S12***: It crystallized in the monoclinic space group *Pc* ($Z=2$) with three molecules of TMZ conformer A (suffix with A, B, C), one molecule of 345THBA, and one water molecule in the asymmetric unit ($Z'=1$). In the asymmetric unit, an amide-amide homo-synthon (N_{6B}-H_{6BA}···O_{2C}: 2.966 Å, N_{6C}–H_{6CA}···O_{2B}: 2.907 Å) is formed between TMZ molecules B and C. 345THBA interacts with TMZ molecule A and B *via* N_{6A}-H_{6AA}···O_3: 3.153 Å and O_7–H_7···O_{2B}: 2.735 Å hydrogen bonds, respectively. The water molecule links 345THBA through O_4–H_4···O_8: 2.550 Å hydrogen bond located in the middle of 345THBA and TMZ, giving additional stability to the structure. These five-member units stack and construct a 3D overlapping structure viewed down the crystallographic c-axis (Fig. 2e).

Supramolecular synthons observed in the cocrystal forms of TMZ with HBA, DHBA, THBA, as well as BZA have been investigated and presented in Scheme 2, at the same time, the conformation adopted by TMZ and predominant synthons in each crystal structure have been summarized and given in Table 3. The same acid-amide hetero-synthon is present in the three methanolate/hydrate forms **S3**, **S7**, and **S8**, thus resulting in an analogous crystal packing pattern. The 3D crystal packings of **S1**, **S3**, **S4**, **S7**, **S8**, **S10**, and **S11** are layered, while **S2**, **S6**, and **S12** show a herringbone-like structure. The 3D crystal arrangements of **S3** and **S4** are also similar, and the main difference between these two forms is that methanol molecules are filled into the cavities formed between TMZ and 24DHBA, connecting them acting as both a hydrogen bond acceptor and a donor. The main differences between forms of **S4** and **S6** lie in the conformation of TMZ and predominant hydrogen-bonded synthons: the primary synthons in **S4** (conformation B adopted by TMZ) are the (carboxyl) O-H···O (amide carbonyl) and (hydroxyl) O-H···N (imidazole) hydrogen bonds, while in **S6** is the (hydroxyl) O-H···O (amide carbonyl), (carboxyl) O-H···N (imidazole), as well as N-H···O, N-H···O hydrogen bonds interrupted by the second molecule of TMZ conformation A. The introduction of the second TMZ conformation A in **S6** influences the overall crystal packing, leading to an overlapping packing pattern, while in **S4** it is a layered 3D structure. The acid-amide hetero-synthon (synthon 1)

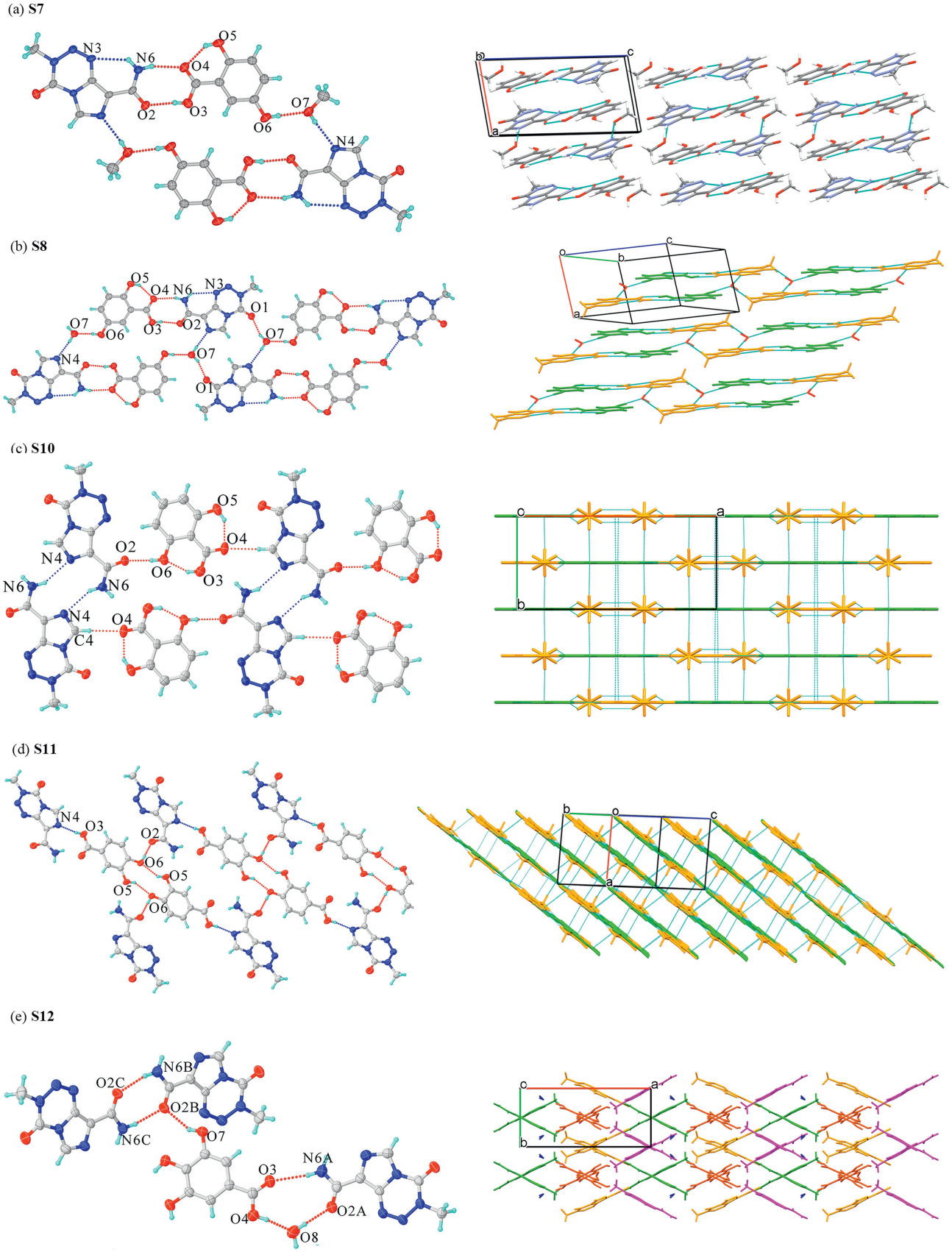

Fig. 2. (a-e) Hydrogen-bonded motifs (left), and the 3D packing structure of the cocrystals **S7**-**S12** (right).

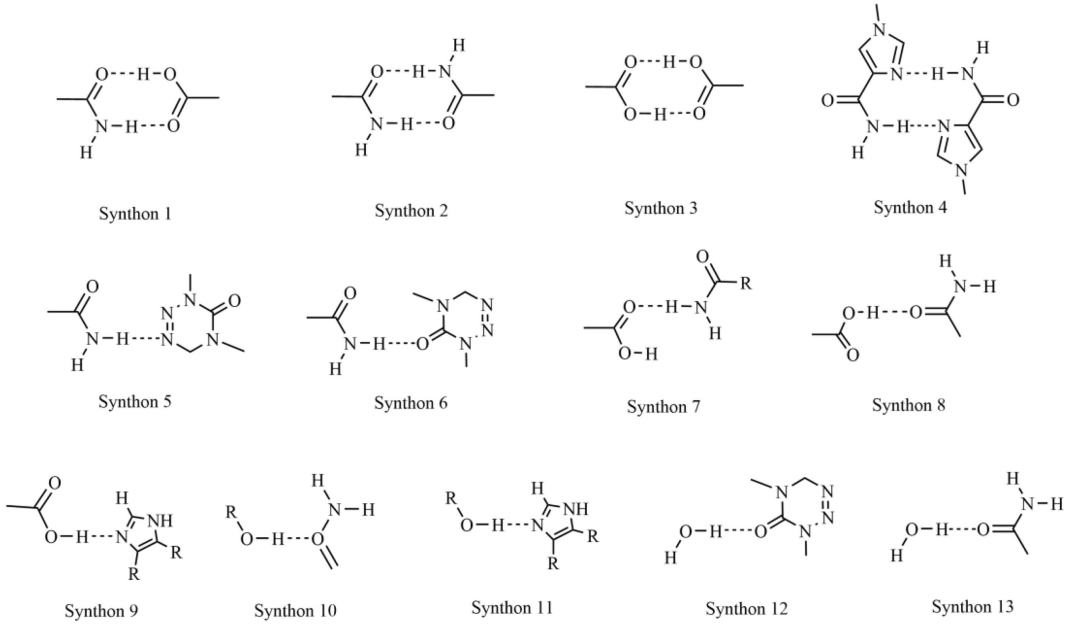

Scheme 2. Supramolecular synthons observed in this study.

and (hydroxyl) O-H···N (imidazole) (synthon 11) are the two synthons that occur most frequently (5 out of 10) in the obtained structures, followed by synthon 10 (4 out of 10): (hydroxyl) O-H···O (amide carbonyl), synthon 7 (3 out of 10): (amide) N-H···O (carbonyl), and synthon 9 (2 out of 10): (carboxylic acid) O-H···N (imidazole), while other hydrogen synthons occur only once. Multiple hydrogen-bond donating and accepting sites on both the API and the CCFs enlarge the spectrum of possible aggregation modes and facilitate the formation of different stoichiometric variations.

In this work, the maxima and minima values of MEPS for TMZ (form 1 used in the experiment), and CCFs (BZA, 3HBA, 24DHBA, 25DHBA, 26DHBA, 34DHBA, 345THBA) were calculated and analyzed (Fig. 3). The positive or negative extreme values reflect the hydrogen bonding donating and accepting abilities. As is evidenced by the MEPS map of CCFs, the global maxima site illustrated in red is mostly distributed over hydrogen connected to hydroxyl groups and the MEPS in the region of the carboxylic hydroxyl group was slightly weaker and the MEPS near the hydrogen bonded to carbon was the weakest. The global maxima area is distributed around the H atoms attached to the *syn*-NH atom, and the global minima region is concentrated around the amide carbonyl O atom. As anticipated, the carboxyl and hydroxyl groups of CCFs and amide hydrogens of TMZ are the main hydrogen bond donors, and carboxyl oxygens of CCFs and amide oxygen of TMZ are the main hydrogen bond acceptors during the cocrystallization, which also resulted in acid-amide heterosynthon being the main robust hydrogen bond. The success rate of MEPS prediction is 87.5% (7 out of 8) when -10 kJ/mol of ΔE value denoting as the threshold in the cocrystallization of TMZ (Table 1).

The appearance or disappearance of polymorph-specific diffraction peaks is indicative of the presence of a novel phase. The experimental and simulated PXRD patterns of TMZ cocrystals (**S1**-**S11**) and the starting components have been plotted in Fig. 4. Firstly, experimental patterns of the bulk powder prepared by the slurry approach are commendably matched with simulated patterns generated from SCXRD data, confirming the accuracy and purity of obtained solid phases. Furthermore, different polymorphic forms of TMZ-24DHBA and TMZ-25DHBA can be controlled by changing the solvent of the crystallization, and different phases were found to crystallize from the same starting components.

The DSC and TG thermograms of TMZ cocrystals (**S1**-**S11**) and the raw materials have been shown in Fig. 5 and Fig. S2 (Supporting information), respectively. It can be seen that TMZ begins to decompose at approximately 200 °C from the TG profile and shows a sharp exothermic peak at 217 °C in the DSC curve. The two methanolate forms **S3** and **S7** undergo a desolvation process showing endothermic peaks at 115 °C and 109 °C in DSC, respectively, supported by the mass loss in ~60–130 °C (exp. 7.15% *vs.* cal. 8.42%) and ~70–140 °C (exp. 7.36% *vs.* cal. 8.42%) in the TG curve. In the case of the hydrate form **S8**, the dehydration processes peak at 137 °C from DSC thermograms, accompanied by the weight loss in the range of ~95–180 °C (exp. 3.96% *vs.* cal. 4.92%) from the TG curve. **S1**, **S2**, and **S10** show an endothermic peak just before the exothermic process, which might be ascribed to a phase transition followed by decomposition, while there is only one exothermic peak in the other 9 cocrystal forms as well as TMZ pure drug. We have also plotted the melting points of CCFs and decomposition temperatures of corresponding cocrystals. It should be noted that the trends of the decomposition points of cocrystals (TMZ-2HBA [30] < **S1** < **S10** < **S2** < **S9** < **S11** < **S6**) are basically consistent with melting points of CCFs (BZA < 2HBA < 26DHBA < 3HBA < 25DHBA < 34DHBA < 24DHBA) from low to high (Table 1).

TMZ suffers from the disadvantage of instability issues associated with decomposition, which is indicated by the color change from white to pink to dark brown [30–32] and the appearance of new PXRD diffraction peaks [31,32] and chromatographic impurity peaks [12,13]. Accelerated stability tests in terms of PXRD patterns (Fig. S3 in Supporting information), HPLC measurements (Fig. S4 in Supporting information), and color comparisons (Fig. S5 in Supporting information) have been performed in this study. Under the conditions of the accelerated stability test, the color of TMZ pure drug turned from white to pink to brown, accompanied by the impurity peak observed in the HPLC chromatogram and undesired peaks found in the PXRD pattern after 3 months, collaboratively suggesting the instability property of TMZ. Fortunately, it should be noted that **S2**, **S4**, **S5**, **S6**, **S8**, **S10**, and **S11** retain their initial crystal form and remain stable for up to 3 months. The stability of TMZ was improved through cocrystallization with phenolic

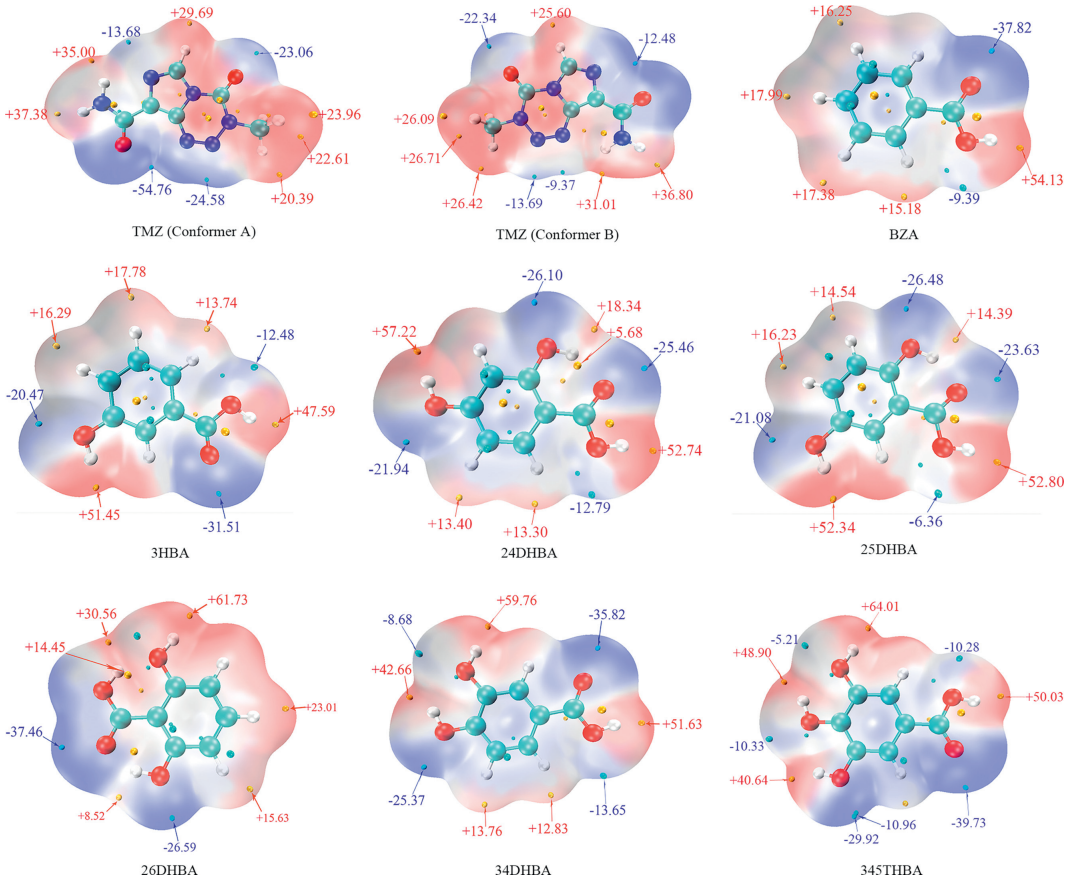

Fig. 3. The positive and negative extreme values (kcal/mol) from MEPS of TMZ (conformers A and B) and CCFs (BZA, 3HBA, 24DHBA, 25DHBA, 26DHBA, 34DHBA, 345THBA).

acids, which could be ascribed to the following two reasons: (i) In the single-component TMZ molecule, the main hydrogen bond is amide-amide homosynthon formed between the two neighboring amide groups: N_6-H_6···O_4 (3.055 Å), N_{12}–H_{12}···O_2 (2.862 Å) (Fig. S6 in Suppporting information), while after cocrystallization, shorter and stronger hydrogen bonds are formed between TMZ and CCFs, with 3HBA in **S2**: acid-amide hetero-synthon (O_3-H_3···O_2: 2.656 Å and N_6-H_{6A}···O_4: 2.969 Å); with 24DHBA in **S4**: O_6-H_6···N_4 (2.878 Å) and O_3-H_3···O_2: (2.590 Å) hydrogen bonds; with 24DHBA in **S6**: O_5-H_5···N_{4B} (2.732 Å) and O_6-H_6···O_{2B} (2.728 Å) hydrogen bonds; with 25DHBA in **S8**: acid-amide hetero-synthon (N_6-H_{6A}···O_4: 2.914 Å and O_3-H_3···O_2: 2.605 Å); with 26DHBA in **S10**: O_6-H_6···O_2 (2.602 Å) hydrogen bond; with 34DHBA in **S11**: O_6-H_6···O_2 (2.569 Å), O_5-H_5···O_6 (2.766 Å), and O_3-H_3···N_4 (2.799 Å) hydrogen bonds. (ii) After cocrystallization, the degradation of TMZ was circumvented as the pH was brought down, and thereby its hydrolytic stability was improved.

S1 was unstable from PXRD analysis under high temperature; the methanolated form **S3** underwent a partial or complete phase transformation to the desolvated form **S4** under the conditions of high temperature and/or high humidity; the methanolated form **S7** converted to the mixture of hydrated form **S8** and desolvated form **S9** at elevated temperature, while completely transformed into **S8** at high humidity, which is consistent with the fact that **S9** is a high-temperature product of **S7**, but **S9** is metastable and easily converted into the hydrated form **S8** even under the storage of the ambient condition. Phase transformations of the three methanolated forms **S3**, **S7**, and **S8** during the accelerated tests confirmed their metastability nature. The hydrated form **S8** remained stable against accelerated conditions, probably because the cavities of the molecular network were filled by appropriate water molecules to achieve a better crystal packing, supported by a higher density of **S8** (1.592 g/cm^3) than **S7** (1.544 g/cm^3) and higher dehydration temperature.

Conversion experiments have long been used to determine the relative thermodynamic stabilities of different polymorphic forms [33]. Among the four forms of TMZ-24DHBA cocrystal, there are several phase transformations as follows: (i) **S3** could convert into **S4** by heating at the temperature of 120 °C for 40 min and/or under the storage of 60 °C for 10 days to remove methanol bound in the crystal lattice (Fig. S7a in Supporting information); (ii) **S4** and **S5** were observed to convert to **S3** by grinding with methanol, while the conversion from **S6** to **S3** only achieved by grinding with methanol together with adding another copy of 24DHBA (Fig. S7c); (iii) grinding **S3**, **S4**, and **S5** with acetonitrile mainly resulted in **S4**, while the resulting phase is exclusively **S6** when the mediated solvent was ethanol (Fig. S7b in Supporting information); (iv) grinding **S6** with another copy of 24DHBA in acetonitrile resulted in a mixture of **S4** and **S6**, while the resulting phase is exclusively **S6** in ethanol. In the cases of three forms of TMZ-25DHBA cocrystal, **S7** and **S9** were found to transform into **S8** under the condition of high humidity or grinding with 95% ethanol, at the same time, the grinding operation of **S8**/**S9** with methanol resulted in **S7**. **S7**/**S8** could change into **S9** by heating at 120/160 °C for 40 min to remove the methanol/water molecules (Fig. S7d). Generally, the proportion of components and the type of solvent are two key factors affecting the resulting form. The diagrams of these phase transformations are shown in Fig. 6, and relative PXRD patterns have been provided in Fig. S7.

In Conclusion, to improve the stability of the antitumor drug TMZ, the crystal engineering technique was employed in this paper. By utilizing the principle of supramolecular synthon and the

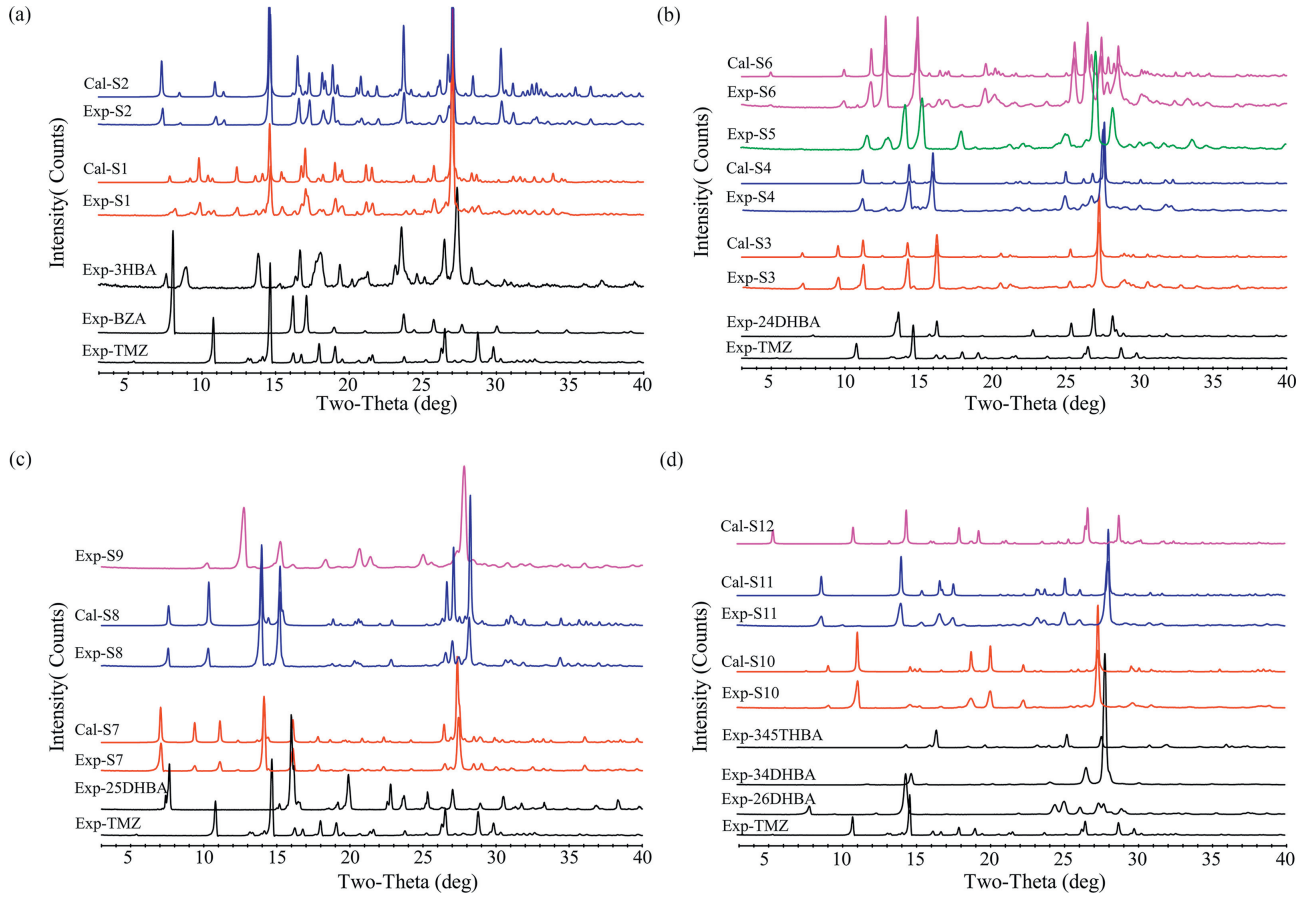

Fig. 4. PXRD patterns of the raw materials, experimental PXRD patterns of cocrystals, and simulated PXRD patterns calculated from SCXRD data. (a) TMZ-BZA (1:1, **S1**), TMZ-3HBA (1:1, **S2**); (b) TMZ-24DHBA-MeOH (1:1:1, **S3**), TMZ-24DHBA (1:1) form A (**S4**), TMZ-24DHBA (1:1) form B (**S5**), TMZ-24DHBA (2:1) (**S6**); (c) TMZ-25DHBA-MeOH (1:1:1, **S7**) TMZ-25DHBA-H_2O (1:1:1, **S8**) TMZ-25DHBA (1:1, **S9**); (d) TMZ-26DHBA (1:1, **S10**), TMZ-34DHBA (1:1, **S11**), TMZ-345THBA (3:1:1, **S12**).

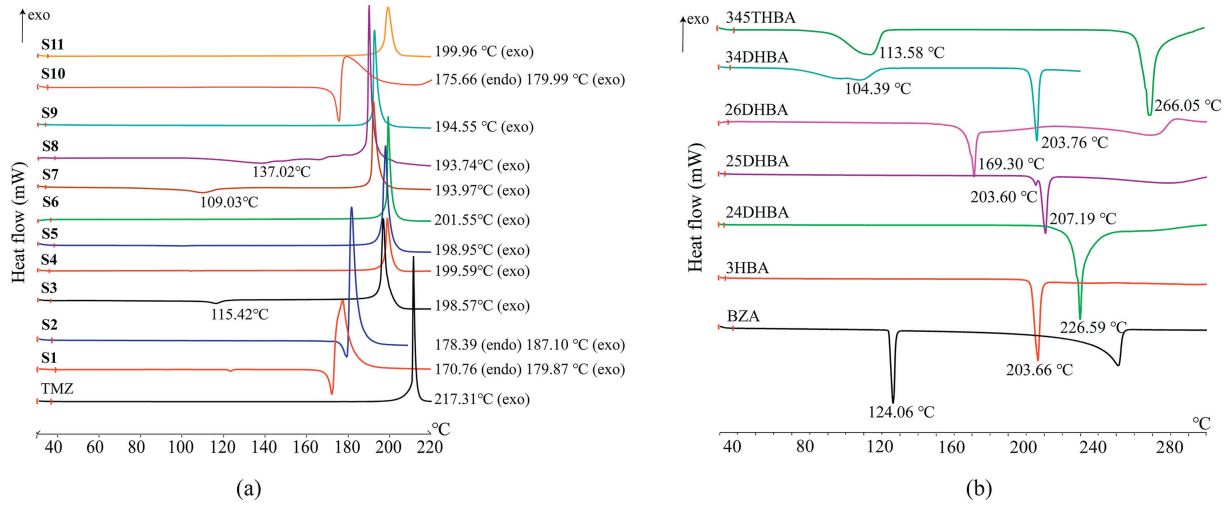

Fig. 5. (a) The DSC thermograms of TMZ and cocrystals, (b) DSC thermograms of CCFs used in this study.

computational method based on MEPS maps, we have designed and synthesized 12 pharmaceutical cocrystal forms of TMZ with benzoic acid and its mono-, di-, and tri–hydroxy derivatives selected from the GRAS list of safe chemicals. The MEPS calculation method is fast enough to be used as a tool for high-throughput virtual screening by evaluating large compound libraries ignoring all aspects of 3D structures, which appears to be a very promising computational tool for improving the efficiency of cocrystal screening. The success rate of the MEPS virtual cocrystal screening method is 87.5% when −10 kJ/mol of ΔE value denoting as the threshold in the cocrystallization of TMZ. The selection of structurally similar compounds as CCFs can also significantly enhance the success rate of experimental screening. The structural analysis implied that -OH- and-COOH-containing aromatic entities are

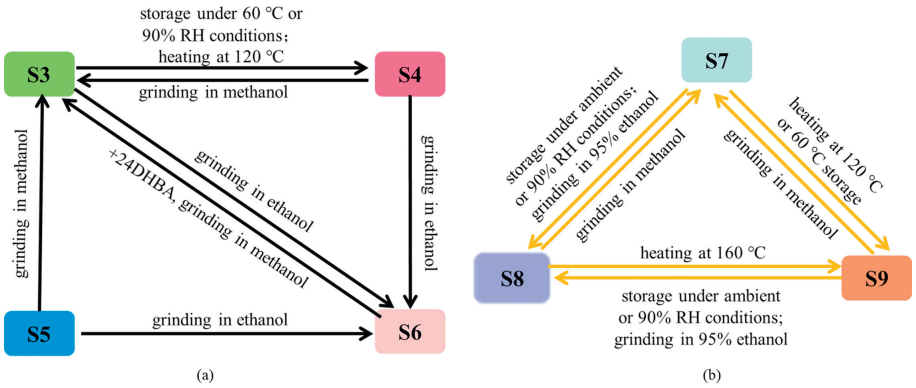

Fig. 6. Schematic diagram of phase transformations of (a) TMZ-24DHBA and (b) TMZ-25DHBA cocrystal forms.

attractive CCFs to TMZ, which deserves further research. Stability tests revealed that **S2**, **S4**, **S5**, **S6**, **S8**, **S10**, and **S11** remained physically and chemically stable for up to 3 months, evidenced and supported by color comparisons, PXRD, and HPLC examinations, which could be ascribed to shorter and stronger hydrogen bonds and more acidic characteristics.

It is difficult to predict the outcome of the cocrystallization process since serendipitous solid forms such as solvates, hydrates, and polymorphs of cocrystals or APIs all are possible products. Ideally, it is necessary to employ different methods and solvents to achieve a maximum output of solid forms. For widespread applications of pharmaceutical cocrystals and to minimize the likelihood of unexpected forms, it is of paramount importance to explore conditions under which specific desired forms can be obtained in the pharmaceutical industries.

Declaration of competing interest

The authors declare that they have no known competing financial interests or personal relationships that could have appeared to influence the work reported in this paper.

Acknowledgments

This work was supported by the Beijing Natural Science Foundation (No. 7222261), CAMS Innovation Fund for Medical Sciences (Nos. 2022-I2M-01-015 and 2022-I2M-JB-010), Key R&D Program of Shan Dong Province (No. 2019JZZY020909), Chinese Pharmacopoeia Commission Drug Standard Promoting Fund (No. 2022Y01).

Supplementary materials

Supplementary material associated with this article can be found, in the online version, at doi:10.1016/j.cclet.2023.109032.

References

[1] G. Yuan, Z. Hui, J. Zhang, Prog. Chem. 22 (2010) 829–836.
[2] H.M. Yu, B.X. Zhang, W.H. Xing, et al., Chin. Chem. Lett. 34 (2023) 107668.
[3] X. Ji, D. Wu, C. Li, et al., Cryst. Growth Des. 22 (2022) 428–440.
[4] H. Fael, R. Barbas, R. Prohens, et al., Pharmaceutics 14 (2021) 49.
[5] R.M. Cruz, T. Boleslavská, J. Beránek, et al. Pharmaceutics 12 (2020) 741.
[6] S. Aitipamula, P.S. Chow, R. Tan, Cryst. Growth Des. 10 (2010) 2229–2238.
[7] Z.Y. Fang, B.X. Zhang, W.H. Xing, et al., Chin. Chem. Lett. 33 (2022) 2159–2164.
[8] T. Ueto, N. Takata, N. Muroyama, et al., Cryst. Growth Des. 12 (2012) 485–494.
[9] S.K. Rai, D. Baidya, A.K. Nangia, CrystEngComm 23 (2021) 5994–6011.
[10] S. Bhattacharya, J. Sameena, B.K. Saha, Cryst. Growth Des. 11 (2011) 905–909.
[11] M.F.G. Stevens, E.S. Newlands, Eur. J. Cancer 29 (1993) 1045–1047.
[12] J.M. Li, X.L. Dai, G.J. Li, T.B. Lu, J.M. Chen, Cryst. Growth Des. 18 (2018) 4270–4274.
[13] J. Wang, X.L. Dai, T.B. Lu, J.M. Chen, Cryst. Growth Des. 21 (2021) 838–846.
[14] N.J. Babu, P. Sanphui, A. Nangia, Chem. Asian J. 7 (2012) 2274–2285.
[15] V.R. Thalladi, B.S. Goud, V.J. Hoy, et al., Chem. Commun. 3 (1996) 401–402.
[16] L.C. Wang, Q.Y. Zheng, Hydrogen Bonding in Supramolecular Crystal Wngineering, Springer Berlin Heidelberg, Germany, 2015, pp. 69–113.
[17] B.J. Denny, R.T. Wheelhouse, M.F.G. Stevens, L.L.H. Tsang, J.A. Slack, BioChem 33 (1994) 9045–9051.
[18] https://www.fda.gov/food/food-ingredients-packaging/generally-recognized-safe-gras. Accessed 5th February, 2023.
[19] Z. Sroka, W. Cisowski, Food Chem. Toxicol. 41 (2013) 753–758.
[20] D. Musumeci, C.A. Hunter, R. Prohens, S. Scuderi, J.F. McCabe, Chem. Sci. 2 (2011) 883–890.
[21] M. Borovina, I. Kodrin, M. Đaković, Cryst. Growth Des. 19 (2019) 1985–1995.
[22] B. Sandhu, S.A. Savage, H. Park, et al., Cryst. Growth Des. 22 (2022) 4105–4114.
[23] D. Meyer, R.V. Berwaer, A.V. Lierde, et al., J. Med. Chem. 35 (1992) 3377–3382.
[24] G.M. Sheldrick, Acta Crystallogr. Sect. A Found. Adv. 71 (2015) 3–8.
[25] G.M. Sheldrick, T.R. Schneider, Methods Enzymol. 277 (1997) 319–343.
[26] M.J. Frisch, G.W. Trucks, H.B. Schlegel, et al., 2016. Gaussian 16, revision A.03; Gaussian, Inc.: Wallingford, CT.
[27] M.M. Lawal, T. Govender, G.E.M. Maguire, G. Kruger, Int. J. Quantum Chem. 118 (2018) e25497.
[28] T. Lu, F. Chen, J. Comput. Chem. 33 (2012) 580–592.
[29] T. Lu, F. Chen, J. Mol. Graph. Model. 38 (2012) 314–323.
[30] A. Nangia, N.J. Babu, P. Sanphui, W.O. Patent, 2011036676 A2, 2011.
[31] O. Braverman, R. Feishtein, A. Weisman, J. Kaspi, U.S. Patent, 0222792 A1, 2006.
[32] Z. Attari, C.M. Rao, L. Kumar, K.B. Koteshwara, Adv. Sci. Lett. 23 (2017) 1841–1845.
[33] S. Aitipamula, A.B.H. Wong, P.S. Chow, R.B.H. Tan, CrystEngComm 14 (2012) 8193–8198.